Storm surge and tidal dissipation in deltaic wetlands

Giovanna Nordio, Sergio Fagherazzi

Department of earth and Environment Boston University, Boston, MA 02215

Abstract

Deltas are complex systems where tidal and riverine signals interact with each other. In river-dominated systems, where river discharge is sufficiently high, tidal amplitude is attenuated and distorted. Here we use wavelet analysis to examine the water level signal in stations located in the Wax Lake delta, part of the Mississippi River Delta in Louisiana, USA. We study the signal attenuation in marshland at different frequency bands, following the propagation of the water level signal from the Gulf of Mexico to innermost stations. During high river discharge, the astronomical tide measured inside the wetlands is reduced of 90%-98% in comparison to the tide measured in Atchafalaya Bay. Storm surge events, largely occurring at lower temporal frequencies, propagate conserving their energy once the signal enters the delta mouth. The river discharge signal, mostly present at frequencies lower than 1.59 μHz, is felt depending on river discharge conditions and the station position within the marshland. Our results suggest that wetlands in the Wax lake Delta act as a low pass filter attenuating tidal components but not the low frequency components of storm surges.

Introduction

River deltas are productive ecosystems, occupying 5% of the global land area. Their high ecological value is related to the extensive wetlands, the rich biodiversity, and underground resources of oil, gas and salts, making them some of the most unique landscapes in the world (Ottinger et al., 2013, Kuenzer et al., 2014). Flat topography, available arable land, fertile alluvial soil, and abundant resources make deltas a preferred location for human settlements (Ottinger et

al., 2013, Kuenzer et al., 2014). River delta vulnerability is connected to humans and climate. The concentration of population and economic activities in deltas cause severe stresses, modifying natural areas with infrastructures, compacting ground, encouraging land subsidence and altering erosion/accretion balance through dam construction (Kuenzer et al., 2014). Moreover, these low-lying deltas are often exposed to floods and storm surges, magnified by climate change (Kuenzer and Renaud, 2012). Many studies have focused on the importance of deltaic wetlands for attenuation of storm surge events (Moller et al., 2014, Stark et al., 2015, Paquier et al., 2016, Yang et al., 2012, Leonardi et al., 2018, Smolders et al., 2015). The loss of wetland areas is detrimental for storm surge attenuation, increasing flooding in coastal communities (Moller et al., 2014). I

The morphological and hydrodynamic complexity of river deltas is related to the river-tide interactions. Fluxes of water, sediments, and nutrients are constantly delivered by both tides and river flow (Ottinger et al., 2013, Kuenzer et al., 2014). Once tides meet the river flow, they are distorted and dissipated due to bottom friction and riverine discharge (Cai et al., 2014, Jay and Flinchem, 1997, Cai et al., 2012, Toffolon and Savenije, 2011, Aubrey and Speer, 1984, Leonardi et al., 2015, Godin 1999). Distortion of tidal waves in shallow water is due to the combination of reflection, refraction, shoaling, and damping (Van der Molen, 1996). The effect of river flow is similar to an increase in bottom friction, by a factor proportional to the ratio between riverine and the tidal discharge (Cai et al., 2014, Cai et al., 2012, Leonardi et al., 2015).

Numerical models have been proposed to study the attenuation of tidal waves in these systems considering bathymetry and river discharge (Cai et al., 2012, Cai et al., 2014) or variations in width and depth of the river (Toffolon and Savenije, 2011). On the contrary, according to Stark et al. (2015), field studies of tidal propagation in marshes are very scarce. Here we use wavelet analysis

to study water elevations data collected by the Coastwide Reference Monitoring System (CRMS) in the Wax Lake delta, Louisiana.

Wavelets transform analysis has already been used to process signals and to better quantify the river-tide-storm interactions in low-lying deltas and estuaries (Leonardi et al., 2015, Spicer et al., 2019, Lee et al. 2018). This mathematical tool can provide significant results over time and space, reconstructing water level signals using complex functions rather than the sinusoidal ones used in Fourier analysis (Lee and Yamamoto,1994, Torrence and Compo, 1998).

Storm and tidal inputs influence different frequency bands in the energy spectrum (Toffoli & Bitner-Gregersen, 2017; Munk 1951). Tidal waves are generated by gravitational attraction and their periods range from 12h to 24h. Surges enhance these oscillations. Storm events along with gravitation attraction generate trans-tidal waves, characterizing by oscillation period higher than 24h. Finally, wind generates waves with period of seconds (Toffoli & Bitner-Gregersen, 2017; Munk 1951). Non-tidal residual, calculated subtracting predicted water levels from observed ones, is composed of an intra-annual seasonal signal, monthly mean sea level anomalies and high-frequency residual representing storm surges due to pressure anomalies and wind setup (Serafin et al., 2017, Spicer et al., 2019, Fernandez-Montblanc et al., 2018, Lee et al 2018).

In this paper we propose an analysis of water level signals recorded by stations located at the end of secondary channels in the Wax Lake delta, part of Mississippi River delta. The Mississippi River Delta, Louisiana, USA, is an example of coastal system quickly degrading. Sea level rise, subsidence, fluid extraction, canal construction, wave erosion, and isolation of most wetlands from sediment supply are considered the major drivers of wetland degradation (Hiatt et al., 2019). On the contrary, Wax Lake delta is considered an actively-prograding sub-delta of the greater Mississippi River delta (Shaw and Mohrig, 2014). Two datasets, one at low river discharge and

the other at high river discharge conditions, are considered. Compared to previous studies, here wavelet transform analysis is used to identify inputs working at different wave frequencies, such as astronomical tide, storm surges, non-tidal residual, and river discharge. For each frequency, we analyze the difference among stations, shedding light on the tide-river interactions.

Study area

The Wax Lake Delta (WLD) is a river delta in the greater Mississippi River Delta (MRD) (LA) (Fig. 1a, b, c). It extends in the Northern part of MRD, receives water from the Mississippi River through a 40 km long 'feeder channel' (Wax Lake Feeder Channel- WLFC) diverted from the Atchafalaya River, and expands in Atchafalaya Bay, in the Gulf of Mexico (Shaw et al., 2013). In 1942, the U.S. Army Corps of Engineers dredged the Wax Lake Outlet (WLO) to redirect around one-third of water of the Atchafalaya River to Atchafalaya Bay (Shaw et al., 2016, Carle et al., 2015). This project was pursued to mitigate the flooding problems in New Orleans and in the lower part of the Mississippi. WLD is the final product of the Atchafalaya River diversion. It receives between 25.6 and 38.4 Mt/yr of sediment, of which a significant amount is silt and clay (Shaw et al., 2013). Recent results have estimated a WLD seaward progression of 270 m/yr between 1980 and 2002 (Shaw et al., 2013). In WLD, two types of distributary channels can be recognized. Primary channels are direct conduits from delta apex to Atchafalaya Bay, while secondary channels connect primary channels to innermost areas, consisting of low-lying wetlands (Shaw et al., 2013).

Major environmental drivers affecting water level dynamics in MRD are river discharge, tidal fluctuations, wind waves, storms, topography and sea-level change (Hiatt et al., 2019). WLD is strongly impacted by river discharge, that influences coastal waters based on the hydrological connectivity between wetlands and river. The seasonal increase in water surface elevation in this

region is mostly due to freshwater discharge coming from the Atchafalaya river and the Intercoastal Water Way (Hiatt et al., 2019). Coastal waters of Louisiana are microtidal (less than 2 m), but tidal ranges considerably vary throughout MRD. WLD is characterized by an average tidal range of 40 cm, with maximum tidal excursion observed during summer and winter solstices and minimum measured during spring and fall equinoxes (Hiatt et al., 2019). The tidal cycle in this region is diurnal, the most significant harmonic constituents are consequently O1 and K1. Semidiurnal constituents M2, S2 and N2 are small along the Gulf of Mexico (Marmer 1954, Hiatt et al. 2019). Climatological forcing seems to have stronger influence than astronomical forcing in WLD. Meteorologically induced water level range can exceed 1 m during the winter months, when the passage of 12-24 h storm events occurs about every 4-7 days. The amplitude of these meteorological fluctuations can be dissipated by friction when they propagate in the innermost wetland areas, where vegetation plays an important role in dissipating water flux energy (Moller et al. 2002, Moller 2006). Hydrodynamic simulations have assessed that wind stress and direction primarily control inundation in WLD. On average, storm surge events reach 25 cm (Hiatt et al., 2019). Between June and November hurricanes and tropical storms affect the MRD area in an infrequent way, causing tremendous damage to coastal communities. The most recent large events were Katrina (August 2005), Rita (September 2005), Gustav and Ike (September 2008) when the surge reached 3 m above m.s.l. along the coast.

Percentage of time wetlands are inundated is between 30 and 50%, and the average flooding depth during inundation is estimated to range from 15 to 20 cm depending on topography (Hiatt et al., 2019). Sea level rise is predicted to be between 0.3 and 2.5 m by 2100 (Hiatt et al., 2019). Wetland plant communities are sensitive to external factors and strong elevation-based zonation is common in these areas (Twilley et al. 2016, Twilley et al. 2019, Bertness and Ellison, 1987). Vegetation in

WLD is typical of freshwater wetlands and swamps according to CRMS (Coastwide Reference Monitoring System) database. *Salix Nigra* and *Colocasia esculenta* are dominant along the natural channels, grasses and forbs at intermediate elevations, *Saggitaria* spp. and *Nelumbo lutea* colonize mudflats, while floating-leaved and submerged aquatic vegetation is present at lowest elevations. Older lobes of the WLD have a mixed community composed of *Colocasia esculenta, Phragmites australis, Polygonum punctatum, Typha spp.*, *Schoenoplectus spp.*, and *Zizaniopsis miliacea* (Twilley et al. 2016, Crale et al. 2013, Visser et al. 1998).

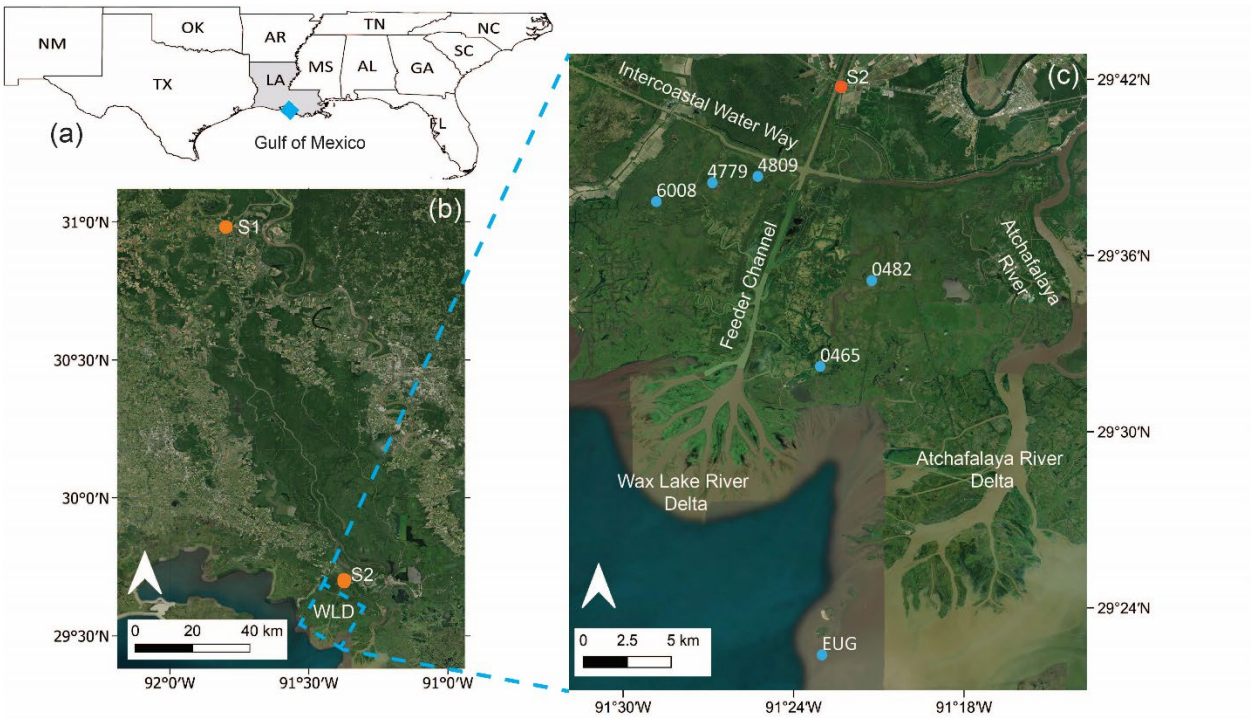

Figure 1: Study area location in the Mississippi River Delta (a). Wax Lake Delta (WLD) and USGS stations S1 and S2 collecting river data locations (b). CRMS sites collecting water level data in marsh channels (0465, 0482, 6008, 4779, 4809), NOAA station (EUG) in Atchafalaya Bay (c).

Methods and Data

Water levels

Five CRMS stations are chosen to study water level attenuation in wetlands (Fig. 1c). The stations are situated at the end of secondary channels in the WLD. Table 1 summarizes the characteristics of each station.

The NOAA station 8764314 Eugene Island (EUG) located in front of the Atchafalaya Delta is considered as the reference for the water levels measured in the Gulf of Mexico. Distance between each CRMS station and the NOAA station is calculated considering the most probable and shortest pathway of water within the channel network (Table 1). GIS (Geographic Information System) and a satellite base-map provided by ESRI (Environmental Systems Research Institute) are used to measure each distance.

Two USGS stations are selected to evaluate the river effect on water levels (Fig 1b, c). The first station, S1, (USGS 07381490 Atchafalaya River at Simmesport S1), 180 km from EUG station, is used to investigate water level frequencies associated to the river flow (Fig. 2b-d), since the tidal signal is very low here. The second station, S2, (USGS 07381590 Wax Lake Outlet at Calumet), 25 km from EUG station, is used to define periods of high and low river discharge (Fig. 3). On average, during winter and spring the river discharge is high around 6000 m^3, while during summer and fall the river discharge is low around 1400 m^3.

Water level data in two time periods are considered to analyze attenuation under low and high river discharge conditions (Fig. 2). The first period from July to September 2017, when river discharge is 2000 m^3 on average (Fig. 2a). The second period from April to June 2019, when river discharge is 7000 m^3 on average (Fig. 2c).

A second water level dataset from July 2019 is considered to investigate water level attenuation during Hurricane Barry. Finally, twenty storm surge events of magnitude ranging from 0.14 to

1.81 m are chosen at the EUG station from 2017 to 2020 (Table. 2). For each station, the storm surge is obtained subtracting the predicted levels from the observed ones, using the T-TIDE program. The storm surges at each location are summarized in Table 2.

Table 1: CRMS stations characteristics

Station	**Marsh elevation [m on NADV88]**	**Distance from NOAA station EUG [km]**	**Marsh vegetation type**
0465	variable floating marsh	23.80	Fresh bulltongue
0482	0.22	32.20	Oligohaline spikerush
6008	-0.18	35.98	Swamp
4779	0.27	33.40	Swamp
4809	0.33	35.75	Swamp

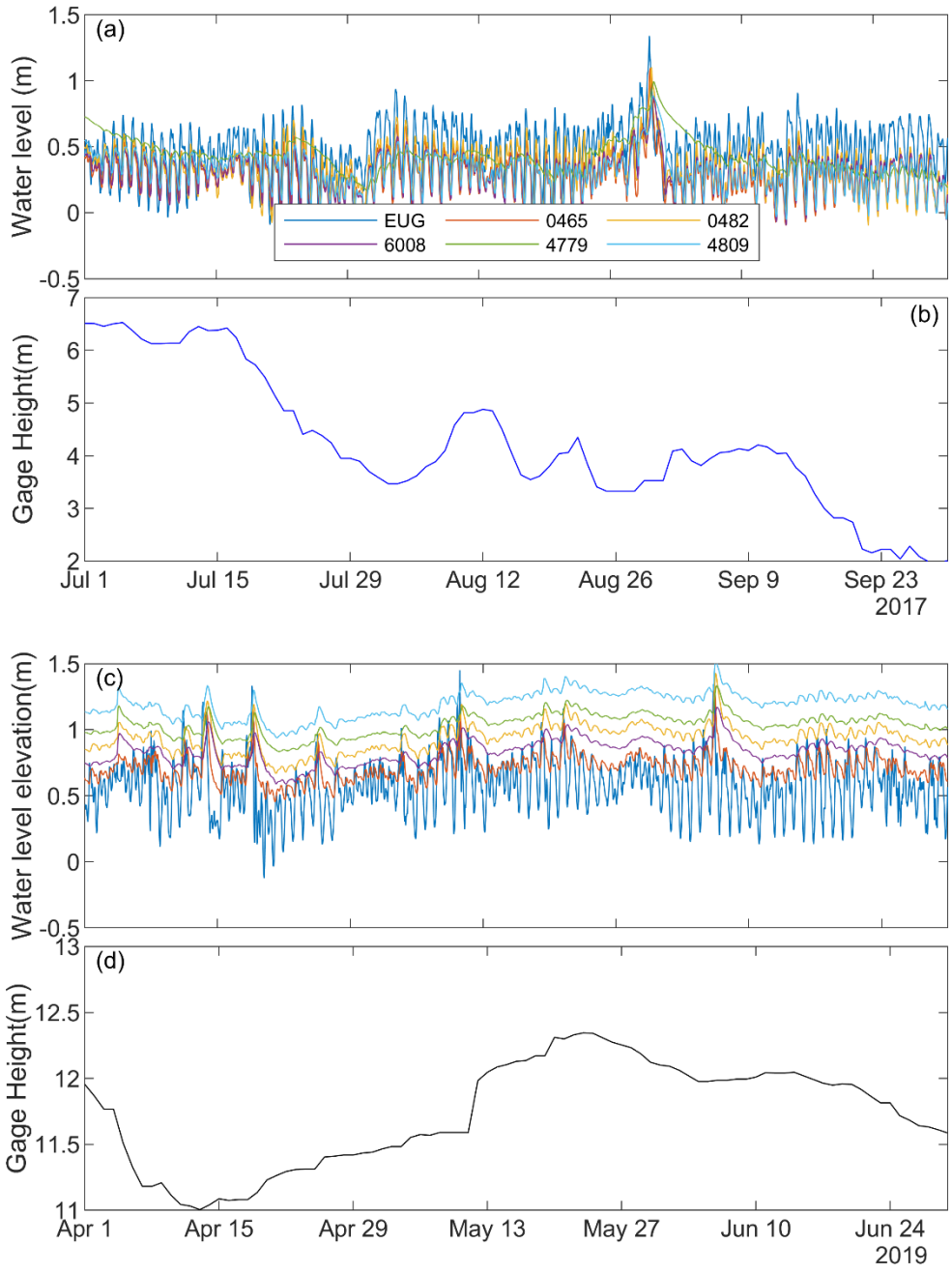

Figure 2: Water levels at different stations at low (a) and high discharge (c) (m above NAVD88). Water level in the Atchafalaya River at Simmesport station (S1) at low (b) and high discharge conditions (d).

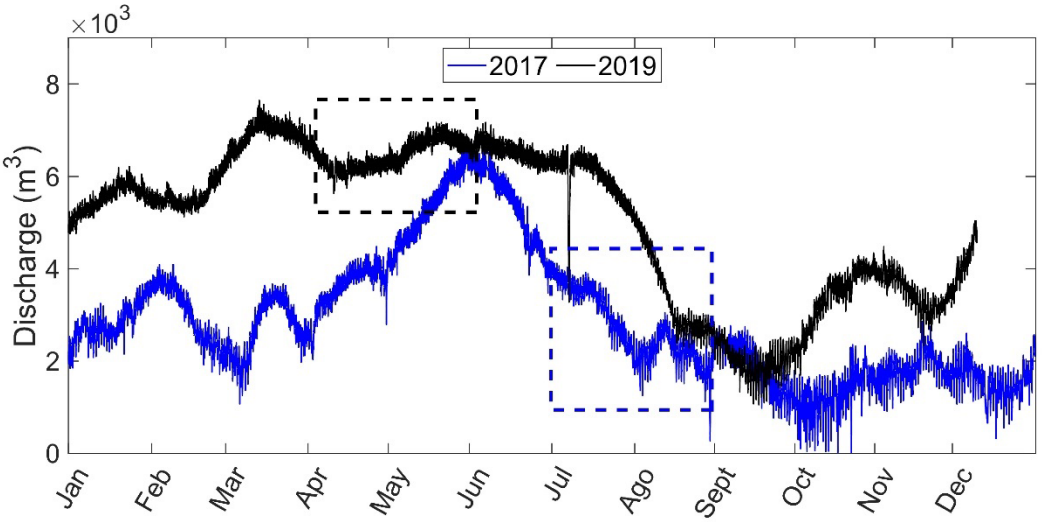

Figure 3: Discharge data in 2017 and 2019 at Wax Lake Outlet at Calumet station (S2). A period of low discharge (July to September) was chosen in 2017 (blue box), while a period of high discharge (April to June) is selected in 2019 (black box).

Table 2: 20 storm surge events selected from 2017 to 2020.

	Time	Discharge	Water level EUG (m)	EUG (m)	0465 (m)	0482 (m)	6008 (m)	4779 (m)	4809 (m)
2017	24-Apr	low	0.23	0.49	0.35	0.32	0.29	0.00	0.24
	12-May	low	0.35	0.35	0.24	0.24	0.14	0.02	0.08
	29-May	high	0.59	1.03	0.35	0.18	0.03	0.02	0.05
	21-Jun	high	0.89	0.27	0.22	0.22	0.18	0.12	0.20
	22-Oct	low	0.91	1.70	0.88	0.82	0.52	NaN	0.44
2018	5-Jun	high	0.14	0.51	0.18	0.19	0.14	0.00	0.16
	17-Jun	high	0.55	0.31	0.26	0.18	0.12	0.06	0.08
	2-Oct	low	0.29	0.10	0.09	0.08	0.03	0.00	0.02
	11-Oct	low	0.64	0.27	0.23	0.18	0.18	0.00	0.19
	14-Oct	low	0.77	0.23	0.19	0.18	0.20	0.05	0.20
2019	4-Apr	high	0.57	0.35	0.04	0.10	0.07	0.01	0.03
	18-Apr	high	0.91	0.50	0.26	0.33	0.25	0.14	0.16
	6-Jun	high	0.78	0.40	0.35	0.33	0.17	0.16	0.16
	13-Jul	high	1.81	2.07	NaN	1.65	1.63	1.20	1.32
	13-Nov	low	0.46	0.47	NaN	0.24	0.24	0.14	0.20
2020	23-Jun	high	0.67	0.55	0.20	0.12	0.08	0.04	0.10
	17-Aug	low	0.26	0.21	0.14	0.14	0.07	0.02	0.09
	21-Sep	low	0.98	0.20	NaN	0.13	0.15	0.05	0.15
	9-Oct	low	1.79	1.20	NaN	0.67	0.51	NaN	0.54
	28-Oct	low	0.68	0.51	NaN	0.35	0.12	NaN	0.13

Harmonic analysis

We perform a classical harmonic analysis using the software T_TIDE. (Pawlowicz et al., 2002). From the observed water levels, the astronomical signal is estimated using complex algebra, and all harmonic components are computed. It is possible to choose among a list of 45 astronomical and 101 shallow-water constituents, matching a specific frequency. For each constituent, amplitude and phase are generated, along with the 95% confidence interval. In our analysis, harmonic analysis is carried out using a NOAA dataset of one year (2018) and a second dataset of three months (January-March 2018) at station EUG (Table 3). Our results well agree with the astronomic constituents reported by NOAA. T_TIDE is successively used to extract the astronomical signal from the observed water levels at each CRMS station. The results are used to analyze the attenuation of the harmonic constituents.

Wavelet transform analysis

Wavelet transform is an analysis tool well suited to study multiscale, nonstationary processes occurring over finite spatial and temporal domains. Wavelet analysis has recently attracted much attention in transient signal analysis, image analysis, communication systems and other signal processing applications (Lee and Yamamoto, 1994, Torrence and Compo, 1998). In comparison to a Fourier analysis, wavelet analysis can provide detailed information of the signal in a time-frequency space, yielding a signal decomposition at different frequencies over time. Wavelet analysis deals with expansion of basic functions not in trigonometric terms like Fourier analysis but using wavelets (Lee and Yamamoto, 1994). Wavelets are generated in forms of translation (identified by a coefficient n) and expansion (identified by a coefficient s) of fixed functions called mother functions. If the mother wavelet respects specific conditions, the wavelet transform on the real signal can be calculated. The wavelet transform can be classified as discrete or continuous

depending on the working domain. In geophysics, Morlet mother wavelet is the most widely used wavelet function in a continuous domain (Jing and Liangsheng, 2000, Lee and Yamamoto, 1994, Lau and Weng, 1995). This wavelet is complex and consists of a plane wave modified by a Gaussian envelope (Lau and Weng, 1995). The advantage of using the Morlet wavelet is its complex nature that can detect both time-dependent amplitude and phase for different frequencies exhibited in the time series (Lau and Weng, 1995). Because the mother wavelet is complex, also the continuous wavelet transform $w_n(s)$, is complex. The *wavelet power spectrum* can be defined as $|w_n(s)^2|$ (Torrence and Compo, 1998, Flinchem and Jay, 2000). It can be visualized in a time-frequency plane where each point has a specific energy. Attenuation of energy between two signals can be visualized in the same time-frequency plane in terms of ratio as:

$$r = \frac{|w2_i(j)^2|}{|w1_i(j)^2|} \qquad (1)$$

where $|w1_i(j)^2|$ and $|w2_i(j)^2|$ are respectively energy of the first and the second signal at specific time i=1,2…N and frequency j=1,2…S. When the ratio is higher than 1 water level energy of the second signal is amplified compared to water level energy of the first signal. Energy associated to a specific frequency s can be calculated as:

$$w_s = \sum_{i=1}^{N} |w_i(s)^2| \qquad (2).$$

Total energy associated to a water level signal can be calculated as:

$$w_{tot} = \sum_{j=1}^{S} \sum_{i=1}^{N} |w_i(j)^2| \qquad (3)$$

Wavelet transform is performed using *Matlab* functions. The goal is to visualize the dominant frequencies representative of the water level signal, recognize the astronomical and meteorological

components and investigate the attenuation of the marine signals (tides and storm surges) going from Atchafalaya Bay (EUG station) to the innermost marshes. Attenuation analysis of river signal is not provided, not having enough stations collecting data along the Atchafalaya River to Wax Lake Delta. We first apply wavelet transform analysis to CRMS and NOAA stations, decomposing the signal in a time-frequency plane. This analysis allows us to recognize storm events and tidal frequencies. We calculate the wavelet power spectrum for each station and provide a measure of energy associated to single values obtained by wavelet transform. According to Toffoli & Bitner-Gregersen (2017) and Munk (1951) we can distinguish different frequency bands. The same analysis is also applied to gage height data collected in S1, to characterize the frequencies of the river signal. In order to measure the attenuation of energy at each station with respect to the energy at the NOAA station (EUG), equation (1) is used, where signal energy, $w2_{n,s}$, at specific time and frequency at each CRMS station is compared to the energy at EUG station, $w1_{n,s}$. The analysis is carried out considering only energy values higher than 0.001 m^2 at EUG station to reduce noise. This ratio provides a measure of energy attenuation for each point in time and frequency. Equation (2) is instead used to estimate signal energy associated to each frequency at each station. Ratio between energy in marshland stations and energy in station EUG is calculated for each frequency band. Equation (3) is finally used to calculate total signal energy in each station. Total signal energy is correlated to both distance and mean water level in each station. An additional analysis is carried out to calculate the attenuation of Hurricane Barry's signal in July 2019.

Table 3: Comparison between amplitude data from NOAA (real data) and calculated using t-tide from a water level signal in a time period of 3 months and one year.

Constituent/ [Frequency (μHz)]		**Amplitude (m)**	**Amplitude difference (m)**	**Phase (deg)**	**Phase difference (deg)**
O1	Real	0.102	-	296.6	-

[11.7]	1 year	0.144	0.006	294.2	2.36
	3 months	0.144	0.022	296.9	6.96
K1 [12.6]	Real	0.157	-	298.2	-
	1 year	0.159	0.006	296.0	2.33
	3 months	0.162	0.017	311.5	5.89
M2 [24.3]	Real	0.102	-	82.8	-
	1 year	0.108	0.004	82.3	1.98
	3 months	0.105	0.009	86.0	4.95
S2 [24.9]	Real	0.036	-	74.2	-
	1 year	0.037	0.004	71.98	6.12
	3 months	0.039	0.008	75.06	13.28
N2 [23.7]	Real	0.036	-	38.5	-
	1 year	0.030	0.004	62.4	7.47
	3 months	0.034	0.008	60.7	13.02

Results

The two datasets considered are characterized by a similar storm surge event reaching a maximum water level of around 1.4 m on NAVD88 (Fig. 2a, c). Water level oscillations are reduced going from EUG to the innermost stations, but are still present in both low and high river discharge conditions (Fig. 2a, c). When the river discharge is high, the average water level increases inland (Fig. 2c). Wavelet transform analysis at low river discharge is shown in Fig. 4. Four frequency bands can be recognized. A first band with frequencies lower than 8.44 μHz, representing weekly, monthly and seasonal oscillations with a period higher than 24hr, a second band between 8.44 μHz and 15.74 μHz, representing tidal oscillations with period around 24 hrs (the tidal harmonics K1 and O1 have frequency 11.61 and 10.76 μHz), a third band between 19.38 and 29.38 μHz representing tidal oscillations with period around 12 hrs (M2, S2 and N2 have frequencies 22.37, 23.15 and 21.94 μHz) and a last band higher than 29.38 μHz, representing hourly oscillations not linked to tides. Note that because the data are collected every hour, the highest frequency that can be recorded is 140 μHz (Nyquist frequency), so that wind waves cannot be captured. In the second and third frequency bands (tidal bands) we can recognize a regular pattern repeating twice a month

where energy minima and maxima follow each other. This pattern is more visible in the second band (diurnal tide) and represents neap and spring modulations.

In low discharge conditions, the energy in the second and third bands is lower in the wetlands, particularly at location 4779 (Fig. 4). The colored area in the first band around 30 of August represents a storm surge, with most energy between frequencies 2 and 4 μHz (period between 3 and 6 days). The attenuation of the tidal frequencies can be better seen in Figure 5, where we plot the ratio between the energy at EUG in Atchafalaya bay and the energy at each wetland location. In this plot we masked areas with an energy at EUG below 0.001 m^2. Both bands 2 and 3 are characterized by ratios below 1, indicating attenuation. The attenuation is very high at 4779, where the tidal energy is basically close to zero. But considerable attenuation is also present at 4809 and 6008. On the contrary, the energy associated to the storm surge event on 30 August 2017 is conserved at almost all stations (ratio close to 1 in Fig. 5) except for station 4779.

Signal attenuation is more significant at high discharge conditions (Fig. 6 and 7). The tide is barely felt when the signal reaches the innermost stations, and the energy ratios are close to zero. The energy associated to the storm surge events in April and June 2019 are attenuated between 30% to 70% at stations 0465 and 4809 (Fig. 7).

The total energy at each frequency is presented in Fig. 8a, b. Energy attenuates going from station EUG to marshland stations in each frequency band. Maximum energy attenuation occurs for diurnal frequencies in both low and high discharge. In high discharge, energy suddenly attenuates from values of 79 m^2 in station EUG to values of 8.3 m^2 in station 0465 (Fig. 8b).

Average attenuation of the signal energy for each frequency band is reported in Fig.8c, d. In high discharge, signal energy is attenuated in each frequency band once signal enters the marshland

(Fig. 8d). at low discharge, the dissipation ratios are higher, indicating less energy dissipation. This is particularly true for the first band, displaying energy conservation (ratio near 1).

Total energy of signal is related to distance of CRMS stations from station EUG (Fig. 9a, b) The energy linearly decreases with distance both at low (R^2= 0.68, p<0.05) and high (R^2= 0.96, p<0.05) discharge, although at high discharge the attenuation is so strong that all the wetlands points are clustered together in Fig. 9b.

Regression analysis conducted on wetland points only at both high and low discharge conditions show a significant correlation between total signal energy and mean water level (R^2= 0.76, p<0.05) (Fig.9c). This result is more evident at high discharge where the high water levels driven by the rivers dissipate most energy.

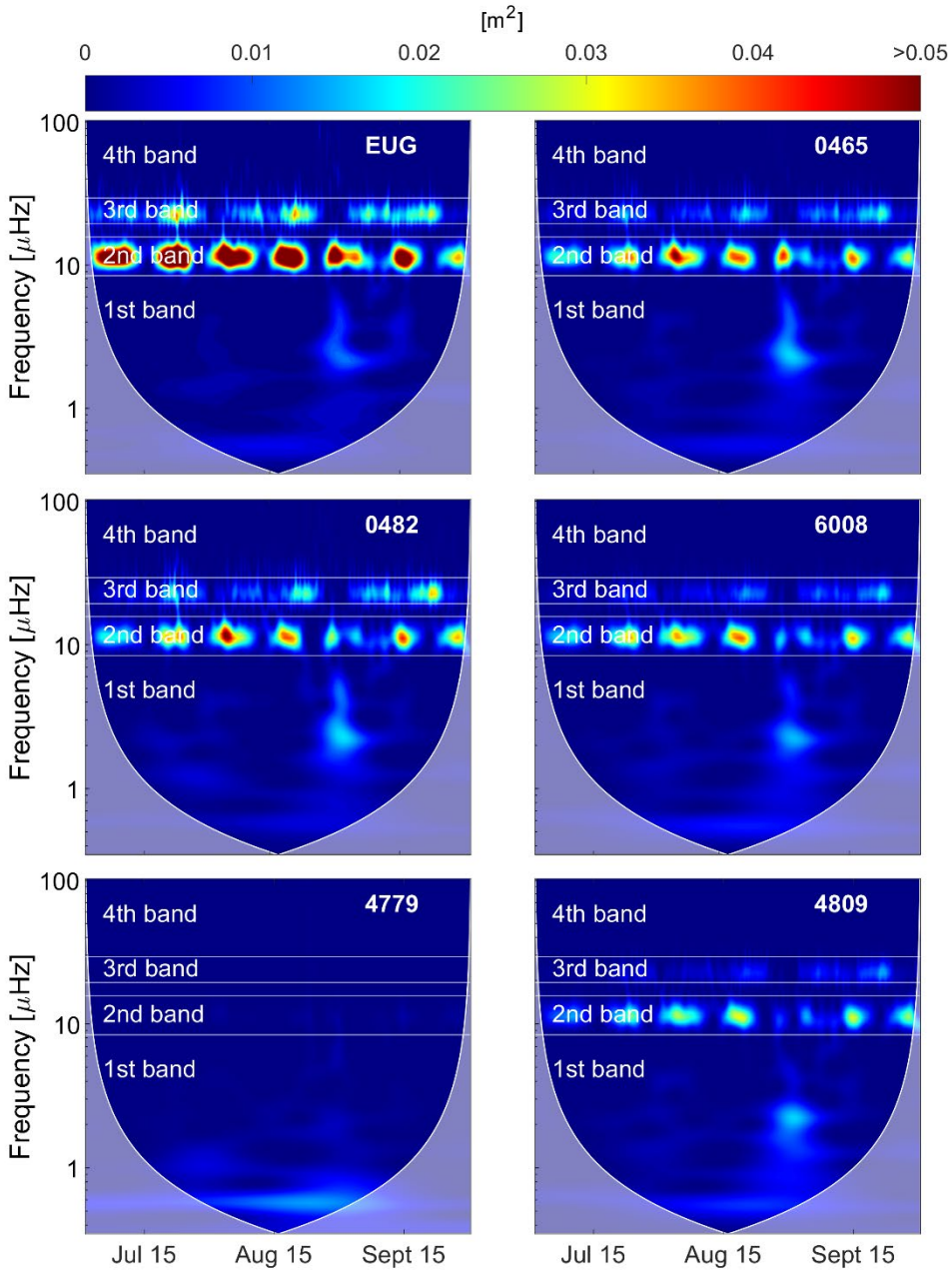

Figure 4: Wavelet power spectrum in low discharge conditions in each station. Higher energy is represented by warmer color, while lower energy by cold colors. Cone of influence define the valid power spectrum region

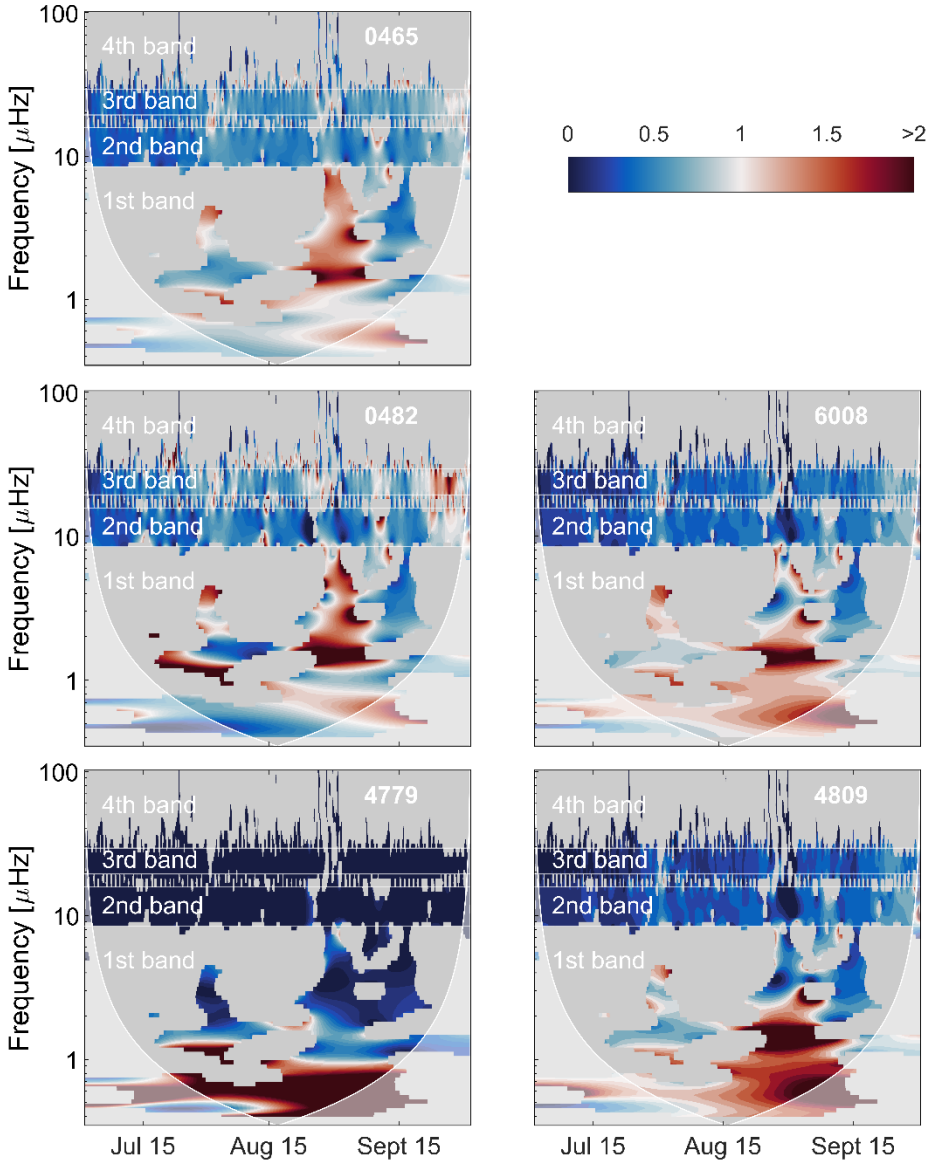

Figure 5: Ratio between energy in each station and energy in EUG station represented in a time-frequency domain using results of wavelet analysis in low discharge conditions. Higher ratios are represented by red color, while lower energy by blue color. Grey regions are excluded from analysis. Cone of influence define the valid power spectrum region.

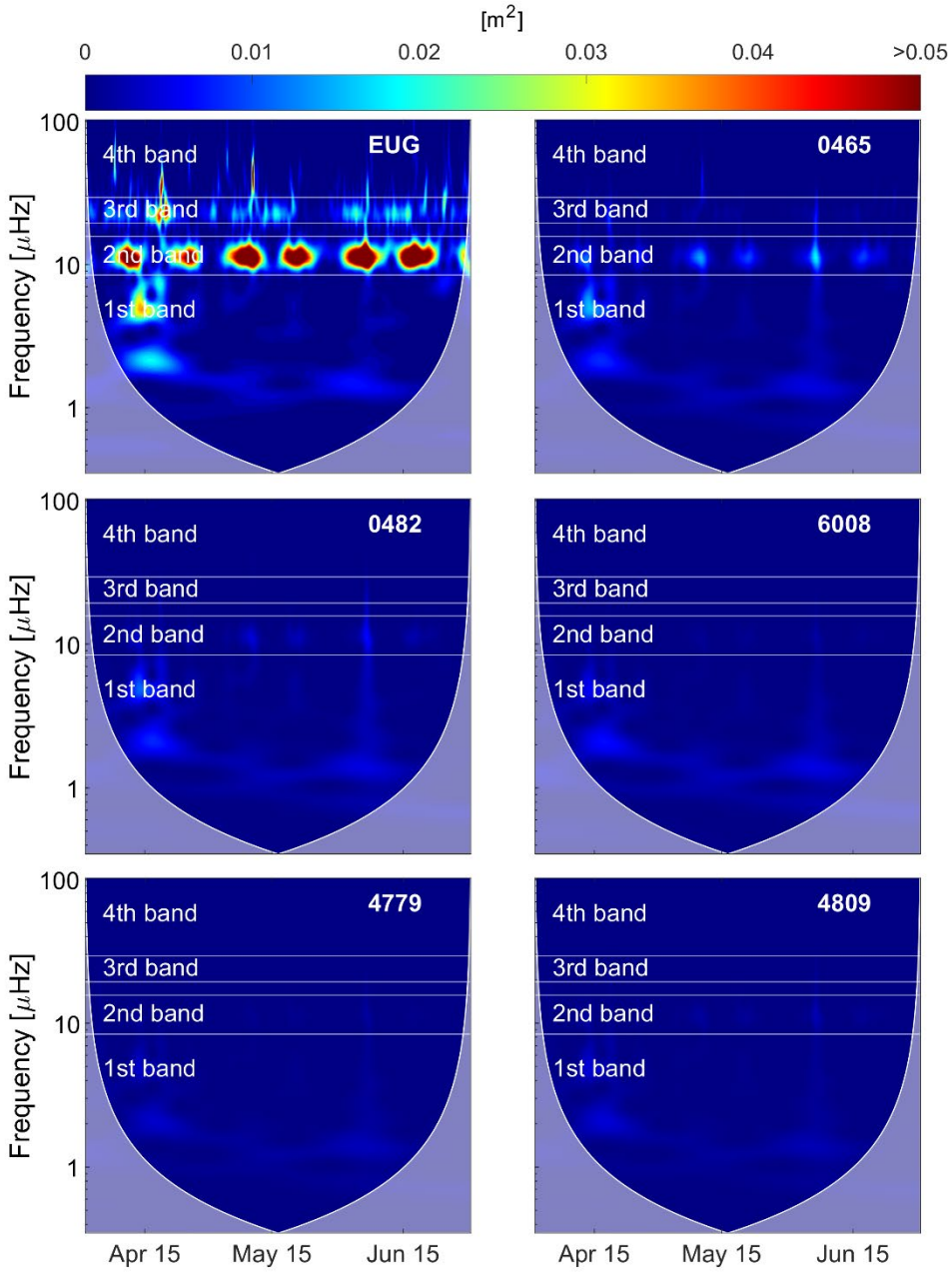

Figure 6: Wavelet power spectrum in high discharge conditions in each station. Higher energy is represented by warmer color, while lower energy by cold colors. Cone of influence define the valid power spectrum region.

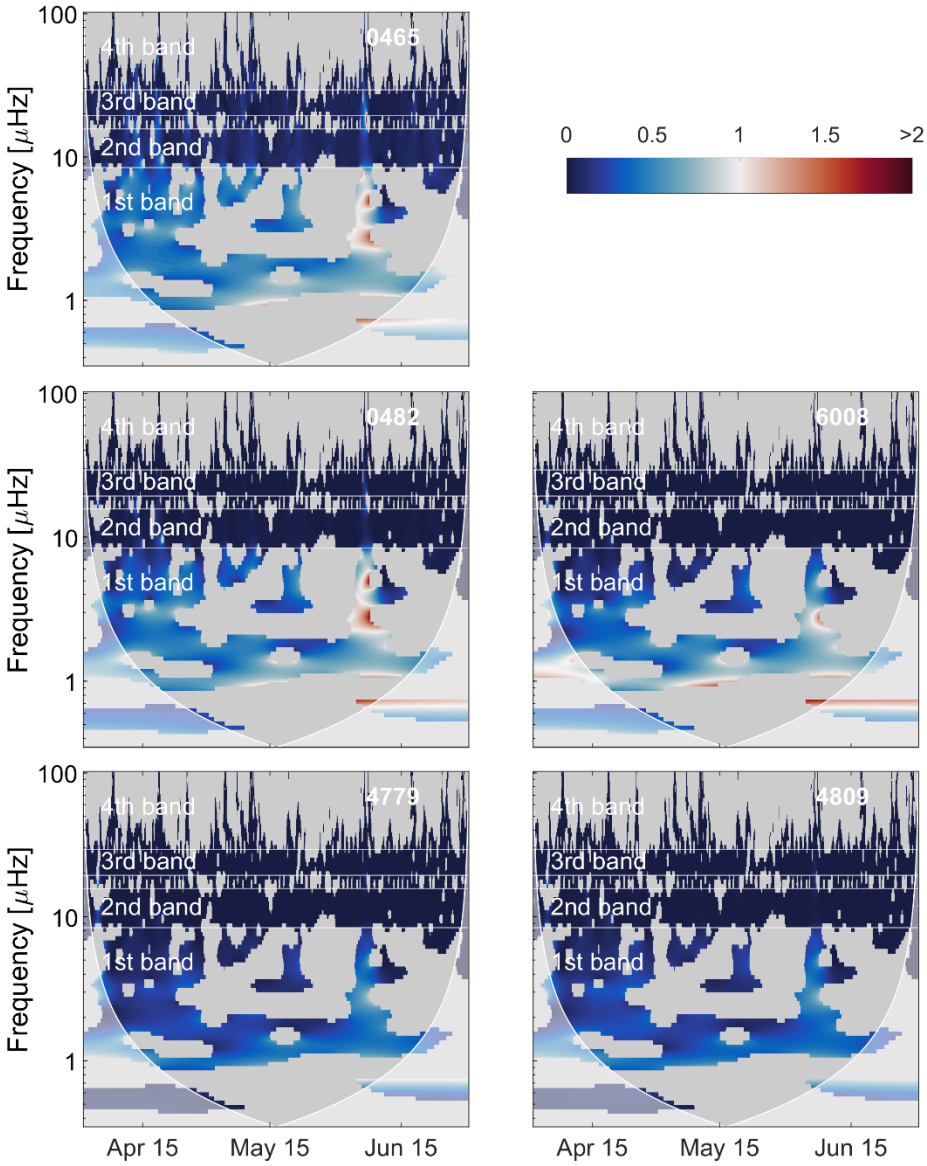

Figure 7: Ratio between energy in each station and energy in EUG station represented in a time-frequency domain using results of wavelet analysis in high discharge conditions. Higher ratios are represented by red color, while lower energy by blue color. Grey regions are excluded from analysis. Cone of influence define the valid power spectrum region.

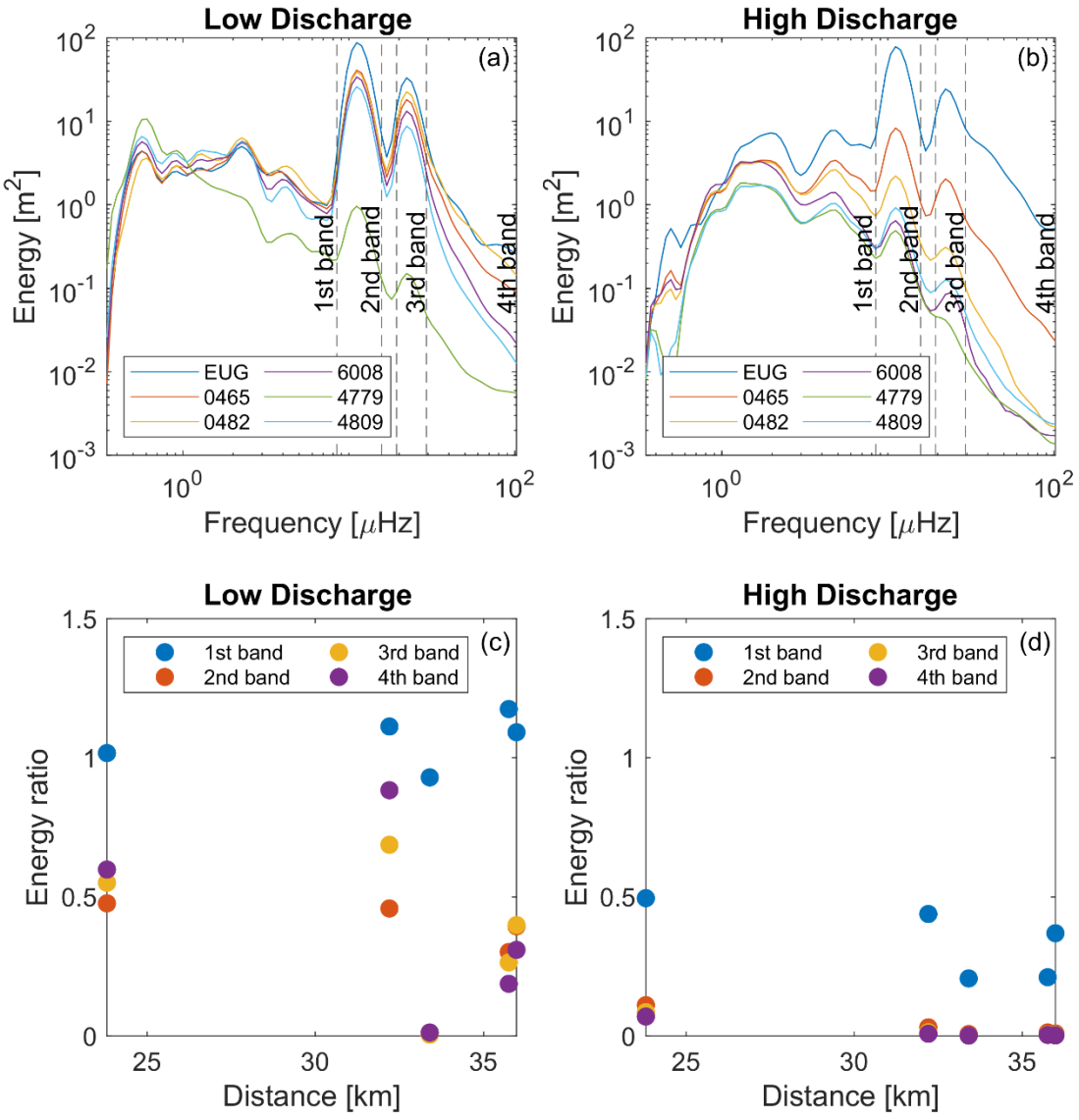

Figure 8: Total energy for each frequency in each station in low discharge (a) and high discharge (b) conditions. Frequency bands are shown. Ratio between total energy in marshland station and total energy in station EUG for each band along the distance of CRMS station from station EUG in low discharge (c) and high discharge (d).

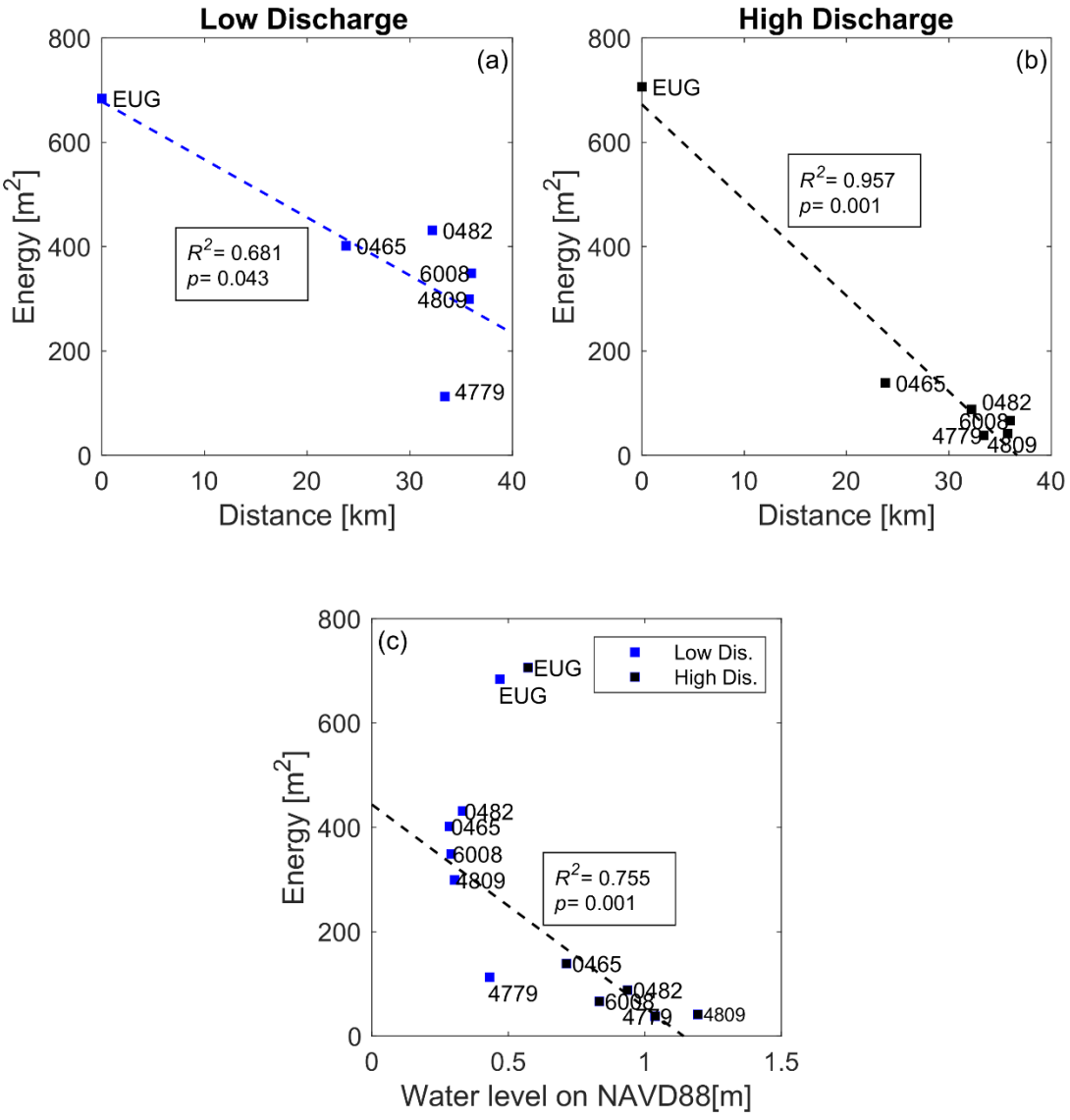

Figure 9: Total energy of signal as a function of distance from EUG station at low (a) and high discharge (b). Total energy of signal trend vs average water level at low (blue points) and high discharge (black points).

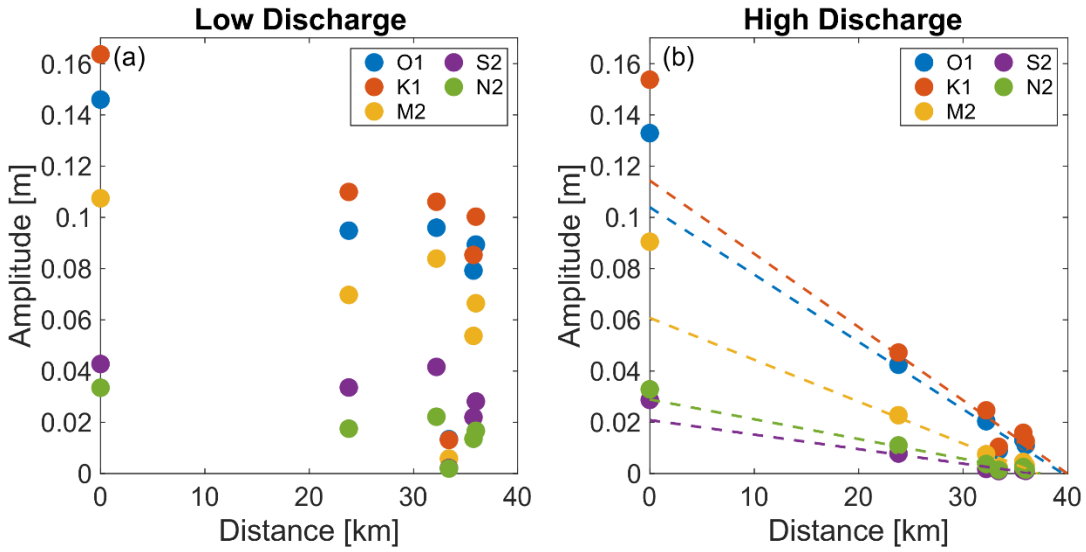

Figure 10: Amplitude trend of O1, K1, M2, S2 and N2 along pathway from EUG station to marsh stations in low (a) and high (b) discharge conditions. Significant regression analysis are represented using dotted lines.

Astronomical harmonics

With the T-Tide package we can better analyze the propagation of each astronomical signal both during low (Fig. 10a) and high river discharge conditions (Fig. 10b). Amplitudes of harmonic constituents vary from 0.16 m for O1 to 0.03 m for N2 at low discharge and from 0.15 m for O1 to 0.02 m for S2 at high discharge. A regression analysis shows a significant correlation between amplitude of each constituents and distance at high discharge ($R^2 > 0.9$, $p < 0.05$) (Fig. 10b).

Storm events

Wavelet transform results are provided for the one-month dataset of July 2019, when Hurricane Berry (13 July 2019) hit the coast (Fig. 11-13). On 13 July 2019 at 12.00 pm water level at station EUG reached 2.14 m. River discharge was high based on USGS data. The peak value of water level got attenuated as the signal entered in the innermost stations (Fig. 11). No data are available

for station 0465 in this period. The energy of the hurricane is mostly concentrated in the first and the second band (diurnal) (Fig. 11). The maximum attenuation involves the diurnal band where tidal energy is present. In the first band, between 1.59 μHz and 8.44 μHz, energy attenuates of 40% from station EUG to station 4779 (Fig. 12). Analysis performed for each frequency band confirms that the attenuation mostly occurred in the second, third and fourth bands (Fig. 13a). Total energy trend is also reported in Fig. 13b.

An additional analysis was done considering twenty different storm events between 2017 and 2020, focusing on the non-tidal surge measured at different stations (Table 2, Fig. 14). Ratios between storm surge effect at marshland stations and at station EUG are calculated to identify attenuation. A global regression analysis suggests that a significant correlation between storm surges and distance is likely to occur when storm surges are higher than 0.3m at station EUG, while for lower surges the attenuation is less.

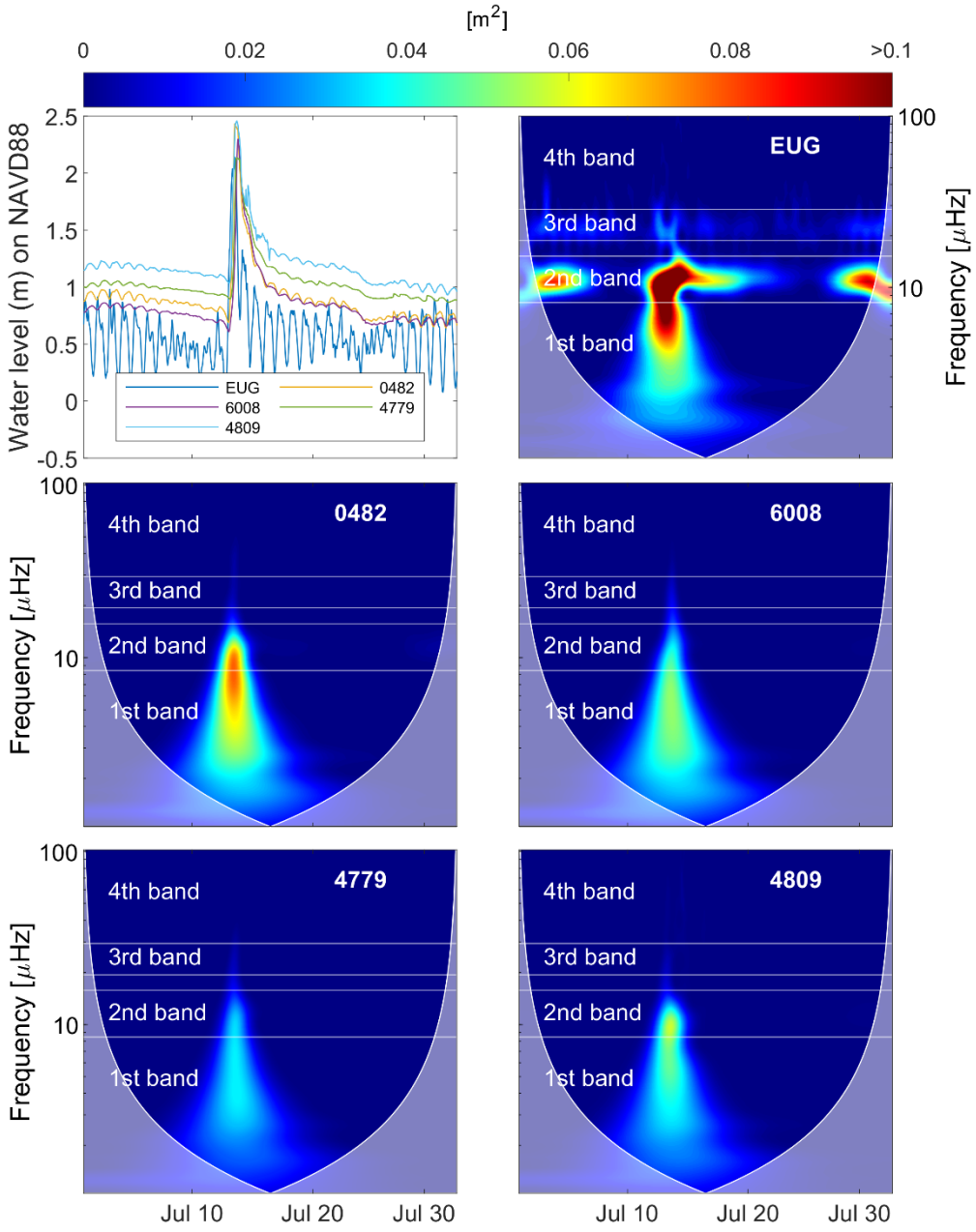

Figure 11: Signal and wavelet power spectrum in July 2019 (Hurricane Barry) in each station. Higher energy is represented by red color, while lower energy by blue color. Cone of influence define the valid power spectrum region.

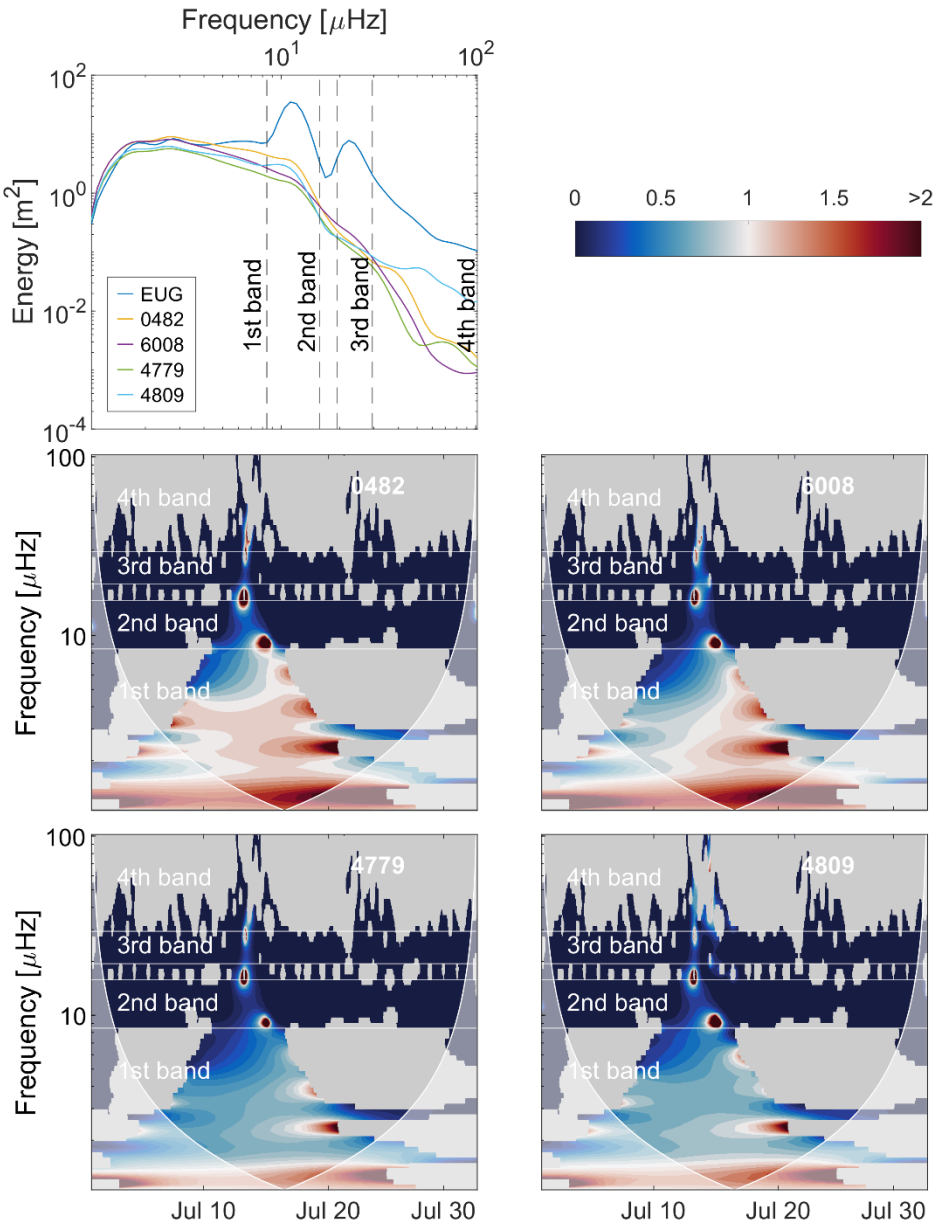

Figure 12: Ratio between energy in each station and energy in EUG station represented in a time-frequency domain using results of wavelet analysis in July 2019 (Hurricane Barry). Higher ratios are represented by red color, while lower energy by blue color. Grey regions are excluded from analysis. Cone of influence define the valid power spectrum region. Energy for each frequency is reported in the first plot.

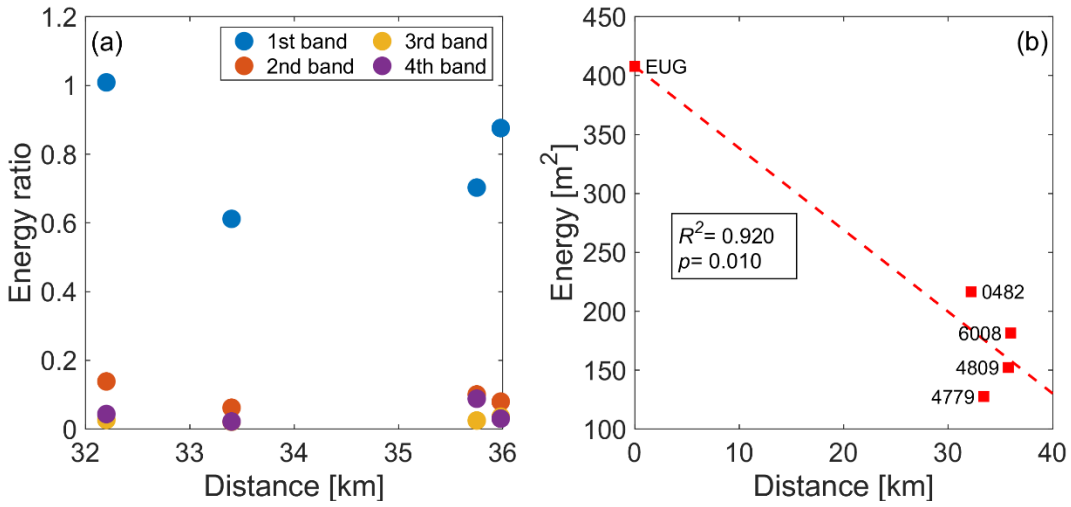

Figure 13: Variation of total energy for each band along the distance of CRMS station from station EUG (a) and total energy of signal trend along distance (b).

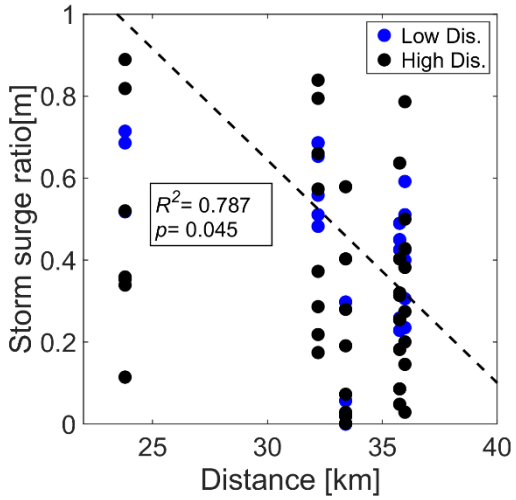

Figure 14: Storm surge ratios trend for 20 events from 2017 to 2020 in low (blue points) and high (black points) discharge conditions along pathway from EUG station to marsh stations. A significant regression line is represented for storm surge at station EUG higher than 0.3 m.

River inputs

As river discharge increases, the water levels in the wetlands are more affected by the fluvial signal. Wavelet analysis performed on the river gage dataset (station S1, Fig. 1) suggests that variations in river water levels mostly occur at low frequencies (< 1.59 µHz) (Fig. 15). Water level measured from the delta mouth to the innermost areas is affected by an amplification of energy at low frequencies in low river discharge conditions (Fig. 4, 5, 8a). The amplification is higher at stations far from the mouth. For frequency lower than 1.59 µHz in the first energy band, energy associated to the matching signal increases from 0.006 m^2 at the EUG station to a maximum of 0.012 m^2 at the station 4779 (Fig. 4). Fig.9a suggests that at station 4779 energy calculated for these frequencies (< 1.59 µHz) reach values 2 times higher (~10 m^2) than at the EUG station (~4 m^2). Therefore stations far from the ocean are more affected by the river signal. During the high discharge period, the amplification effect due to the river is not felt (Fig. 5, 6, 8b), likely because the water level in the river is almost constant (Fig. 2d).

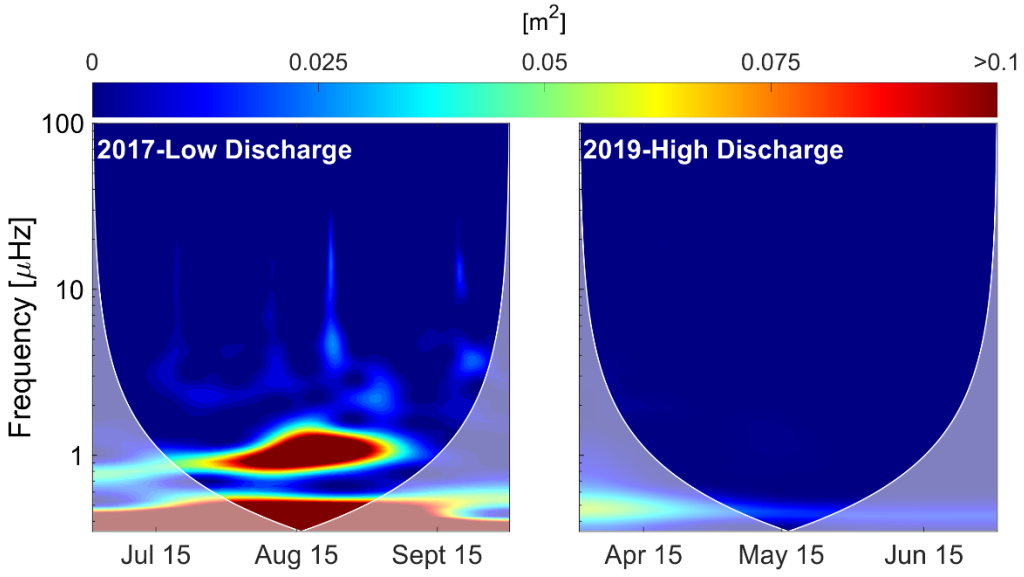

Figure 15: Wavelet power spectrum at low and high discharge conditions at the Atchafalaya River station at Simmesport (S1). Higher energy is represented by warmer color, while lower energy by cold colors. Cone of influence define the valid power spectrum region.

Discussion

The water level signal varies within the marshland. This occurs because WLD is a complex system where astronomical, storm surge and river inputs influence each other. Astronomical signal is felt in the diurnal and semidiurnal frequency bands (Wolanski & Elliott, 2015), the non-tidal components of storm surges is concentrated at frequencies lower than 8.44 μHz, but there is also substantial energy in the tidal frequencies (Spicer et al., 2019). The river influence is felt at low frequencies below 1.59 μHz (Fig. 15). Once the marine signal (tides and storm surges) propagates in the marshland, the energy is reduced (Fig. 9a, b, 13b). At low discharge, the energy of the astronomical signal is reduced by half when the tide reaches the first station 0465, and then is maintained at the same level in the innermost stations. At high discharge the attenuation is larger, leading to a 90% dissipation just in the first station closer to the delta mouth, and to a complete dissipation at station 4779. Diurnal components are more attenuated.

In low discharge conditions, in station 4779 astronomical amplitudes are distorted and smaller (Fig. 2a), and astronomical signal energy (Fig. 4-5) is totally dissipated due to its position. This station is directly connected to the intercoastal water way through a little channel, and the river signal in the intercoastal water way might dominate the tides. The strongest river effect in this station is mostly felt at low river discharge due to high river energy at frequencies lower than 1.59 μHz.

At high river discharge, the water levels of all stations are higher, and cause dissipation of tidal energy entering the delta mouth (Fig. 9c). In an estuary dominated by tidal action, the astronomical

signal can propagate upstream (Leonardi et al., 2015, Mao et al. 2004). This occurs when river discharge is sufficiently low, and consequently there is a low damping coefficient. As river discharge increases, reaching conditions of unidirectional flow, upstream propagation area decreases and damping coefficient increases, causing a significant reduction in tidal amplitudes and tidal prism (Cai et al., 2014, Cai et al., 2012, Leonardi et al., 2015).

Water level energy measured between 1.59 μHz and 8.44 μHz is mostly associated to meteorological events. At these frequencies trans-tidal waves can be recognized (Toffoli & Bitner-Gregersen, 2017; Munk 1951). This energy is conserved in the marshland stations in low discharge conditions. In high discharge the energy is progressively attenuated from station EUG to station 4779. Energy at period lower than semidiurnal (fourth band) is produced by winds and attenuates in a way similar to the energy in the tidal frequencies. Small storm surges are only slightly attenuated in the innermost stations, while the signal of more energetic events like hurricanes seems more attenuated.

Dissipation of tidal signal and storm waves in wetlands are related to many factors. The volume of water that can be stored in a marsh can affect storm surge propagation, particularly when the time to fill the wetland area is shorter than the storm surge duration (Stark et al. 2015). In this case the storage area fills before storm surge propagation stops.

Our results have important implications for wetland ecosystems and the resilience of deltas. Overall, marsh dissipation acts on tidal inputs rather than storm surges. Meteorological inputs originate long waves that are able to propagate until the innermost stations. This is important for sediment transport to the marshland (Warner at al. 2008) and therefore vital for marsh survival (Christiansen et al. 2000, Kirwan et al. 2016).

Because of tidal dissipation, variations in water levels are mainly driven by storms in the inner wetlands. This is particularly true when the river discharge is high. Variations in water levels drive fluxes of water, nutrients, and sediments to the wetlands (Fagherazzi et al., 2013), as a result of tidal dumping, the fluxes are more intermittent and do not follow a regular pattern, affecting vegetation. The lack of daily water level oscillations reduces subaerial periods, possibly selecting for vegetation species that can survive long hydroperiods. Reduced tidal fluxes could also diminish the input of sediments to the wetland interior, with accretion only occurring during storms or river flood events.

Our results suggest that wetlands in the WLD act as low pass filter, damping tidal oscillations but with limited dissipation of storm surges. This dynamic would therefore reduce the buffering effect of wetlands against storm inundation. However, even a reduction in tidal signal could provide some protection, since often the worst flooding events are caused by the compound effect of storm surges and high tides.

Conclusions

Overall tides are attenuated when travelling from the coastal ocean to the wetlands interior. At low river discharge, when the WLD is tidally dominated, the attenuation is less. At high river discharge, the tidal semi-diurnal and diurnal frequencies are dissipated of 90% once the signal reaches the first stations closer to the delta mouth. Tidal signal is not more felt at stations far from the WLD mouth.

The river signal affects water levels at low frequency (< 1.59 μHz). If the discharge is low, the river signal is detected at stations farthest from the WLD mouth. During period with constant discharge, the river signal is not felt.

Frequencies lower than 8.44 μHz are non-tidal residuals driven by storm surge events. The energy at these frequencies is conserved in the marshland both for small and large events (e.g. hurricanes). We conclude that the deltaic wetlands in the WLD act as a low pass filter, dissipating tidal components but not the low frequency components of storm surges and hurricanes.

Acknowledgements

We want to thank … for help in analyzing the data. The research was partly supported by NASA Delta-X project (Science Mission Directorate's Earth Science Division through the Earth Venture Suborbital-3 Program NNH17ZDA001N-EVS3) and by the USA National Science Foundation (NSF) Awards 1637630 (PIE LTER) and 1832221 (VCR LTER).

References

- Aubrey, D. G., & Speer, P. E. (1985). A study of non-linear tidal propagation in shallow inlet/estuarine systems Part I: Observations. *Estuarine, Coastal and Shelf Science*, *21*(2), 185-205.
- Bertness, M. D., & Ellison, A. M. (1987). Determinants of pattern in a New England salt marsh plant community. *Ecological Monographs*, *57*(2), 129-147.
- Cai, H., Savenije, H. H. G., & Jiang, C. (2014). Analytical approach for predicting fresh water discharge in an estuary based on tidal water level observations. *Hydrology and Earth System Sciences*, *18*(10), 4153-4168.
- Cai, H., Savenije, H. H. G., & Toffolon, M. (2014). Linking the river to the estuary: influence of river discharge on tidal damping. *Hydrology and Earth System Sciences*, *18*(1), 287-304.
- Cai, H., Savenije, H. H., Yang, Q., Ou, S., & Lei, Y. (2012). Influence of river discharge and dredging on tidal wave propagation: Modaomen Estuary case. *Journal of Hydraulic Engineering*, *138*(10), 885-896.
- Carle, M. V., Sasser, C. E., & Roberts, H. H. (2015). Accretion and vegetation community change in the Wax Lake Delta following the historic 2011 Mississippi River flood. *Journal of Coastal Research*, *31*(3), 569-587.

- Christiansen, T., Wiberg, P. L., & Milligan, T. G. (2000). Flow and sediment transport on a tidal salt marsh surface. *Estuarine, Coastal and Shelf Science*, *50*(3), 315-331.
- Fagherazzi, S., Wiberg, P.L., Temmerman, S., Struyf, E., Zhao, Y. and Raymond, P.A., 2013. Fluxes of water, sediments, and biogeochemical compounds in salt marshes. *Ecological Processes*, 2(1), pp.1-16.
- Fernández-Montblanc, T., Vousdoukas, M. I., Ciavola, P., Voukouvalas, E., Mentaschi, L., Breyiannis, G., ... & Salamon, P. (2019). Towards robust pan-European storm surge forecasting. *Ocean Modelling*, *133*, 129-144.
- Flinchem, E. P., & Jay, D. A. (2000). An introduction to wavelet transform tidal analysis methods. *Estuarine, Coastal and Shelf Science*, *51*(2), 177-200.
- Godin
- Hiatt, M., Snedden, G., Day, J. W., Rohli, R. V., Nyman, J. A., Lane, R., & Sharp, L. A. (2019). Drivers and impacts of water level fluctuations in the Mississippi River delta: Implications for delta restoration. *Estuarine, Coastal and Shelf Science*, *224*, 117-137.
- Jay, D. A., & Flinchem, E. P. (1997). Interaction of fluctuating river flow with a barotropic tide: A demonstration of wavelet tidal analysis methods. *Journal of Geophysical Research: Oceans*, *102*(C3), 5705-5720.
- Kirwan, M. L., Temmerman, S., Skeehan, E. E., Guntenspergen, G. R., & Fagherazzi, S. (2016). Overestimation of marsh vulnerability to sea level rise. *Nature Climate Change*, *6*(3), 253-260.
- Kuenzer, C., & Renaud, F. G. (2012). Climate and environmental change in river deltas globally: expected impacts, resilience, and adaptation. In *The Mekong Delta System* (pp. 7-46). Springer, Dordrecht.
- Künzer, C., Ottinger, M., Liu, G., Sun, B., Baumhauer, R., & Dech, S. (2014). Earth observation-based coastal zone monitoring of the Yellow River Delta: Dynamics in China's second largest oil producing region over four decades. *Applied Geography*, *55*, 92-107.
- Lau, K. M., & Weng, H. (1995). Climate signal detection using wavelet transform: How to make a time series sing. *Bulletin of the American meteorological society*, *76*(12), 2391-2402.
- Lee, D. T., & Yamamoto, A. (1994). Wavelet analysis: theory and applications. *Hewlett Packard journal*, *45*, 44-44.
- Lee, M., You, Y., Kim, S., Kim, K. T., & Kim, H. S. (2018). Decomposition of water level time series of a tidal river into tide, wave and rainfall-runoff components. *Water*, *10*(11), 1568.
- Leonardi, N., Carnacina, I., Donatelli, C., Ganju, N. K., Plater, A. J., Schuerch, M., & Temmerman, S. (2018). Dynamic interactions between coastal storms and salt marshes: A review. *Geomorphology*, *301*, 92-107.
- Leonardi, N., Kolker, A. S., & Fagherazzi, S. (2015). Interplay between river discharge and tides in a delta distributary. *Advances in Water Resources*, *80*, 69-78.
- Lin, J., & Qu, L. (2000). Feature extraction based on Morlet wavelet and its application for mechanical fault diagnosis. *Journal of sound and vibration*, *234*(1), 135-148.
- Mao, Q., Shi, P., Yin, K., Gan, J., & Qi, Y. (2004). Tides and tidal currents in the Pearl River Estuary. *Continental Shelf Research*, *24*(16), 1797-1808.
- Marmer, H. A. (1954). Tides and sea level in the Gulf of Mexico. *US Fish Wildl. Serv. Fish. Bull*, *55*(89), 101-118.
- Möller, I. (2006). Quantifying saltmarsh vegetation and its effect on wave height dissipation: Results from a UK East coast saltmarsh. *Estuarine, Coastal and Shelf Science*, *69*(3-4), 337-351.
- Möller, I., & Spencer, T. (2002). Wave dissipation over macro-tidal saltmarshes: Effects of marsh edge typology and vegetation change. *Journal of Coastal Research*, (36), 506-521.

- Möller, I., Kudella, M., Rupprecht, F., Spencer, T., Paul, M., Van Wesenbeeck, B. K., ... & Schimmels, S. (2014). Wave attenuation over coastal salt marshes under storm surge conditions. *Nature Geoscience*, *7*(10), 727-731.
- Munk, W. H. (1951). *Origin and generation of waves*. Scripps Institution of Oceanography La Jolla Calif.
- Ottinger, M., Kuenzer, C., Liu, G., Wang, S., & Dech, S. (2013). Monitoring land cover dynamics in the Yellow River Delta from 1995 to 2010 based on Landsat 5 TM. *Applied Geography*, *44*, 53-68.
- Paquier, A. E., Haddad, J., Lawler, S., & Ferreira, C. M. (2017). Quantification of the attenuation of storm surge components by a coastal wetland of the US Mid Atlantic. *Estuaries and Coasts*, *40*(4), 930-946.
- Pawlowicz, R., Beardsley, B., & Lentz, S. (2002). Classical tidal harmonic analysis including error estimates in MATLAB using T_TIDE. *Computers & Geosciences*, *28*(8), 929-937.
- Serafin, K. A., Ruggiero, P., & Stockdon, H. F. (2017). The relative contribution of waves, tides, and nontidal residuals to extreme total water levels on US West Coast sandy beaches. *Geophysical Research Letters*, *44*(4), 1839-1847.
- Shaw, J. B., & Mohrig, D. (2014). The importance of erosion in distributary channel network growth, Wax Lake Delta, Louisiana, USA. *Geology*, *42*(1), 31-34.
- Shaw, J. B., Ayoub, F., Jones, C. E., Lamb, M. P., Holt, B., Wagner, R. W., ... & Mohrig, D. (2016). Airborne radar imaging of subaqueous channel evolution in Wax Lake Delta, Louisiana, USA. *Geophysical Research Letters*, *43*(10), 5035-5042.
- Shaw, J. B., Mohrig, D., & Whitman, S. K. (2013). The morphology and evolution of channels on the Wax Lake Delta, Louisiana, USA. *Journal of Geophysical Research: Earth Surface*, *118*(3), 1562-1584.
- Smolders, S., Plancke, Y., Ides, S., Meire, P., & Temmerman, S. (2015). Role of intertidal wetlands for tidal and storm tide attenuation along a confined estuary: a model study. *Natural Hazards and Earth System Sciences*, *15*(7), 1659-1675.
- Spicer, P., Huguenard, K., Ross, L., & Rickard, L. N. (2019). High-Frequency Tide-Surge-River Interaction in Estuaries: Causes and Implications for Coastal Flooding. *Journal of Geophysical Research: Oceans*, *124*(12), 9517-9530.
- Stark, J., Van Oyen, T., Meire, P., & Temmerman, S. (2015). Observations of tidal and storm surge attenuation in a large tidal marsh. *Limnology and Oceanography*, *60*(4), 1371-1381.
- Toffoli, A., & Bitner-Gregersen, E. M. (2017). Types of ocean surface waves, wave classification. *Encyclopedia of Maritime and Offshore Engineering*, 1-8.
- Toffolon, M., & Savenije, H. H. (2011). Revisiting linearized one-dimensional tidal propagation. *Journal of Geophysical Research: Oceans*, *116*(C7).
- Torrence, C., & Compo, G. P. (1998). A practical guide to wavelet analysis. *Bulletin of the American Meteorological society*, *79*(1), 61-78.
- Twilley, R. R., Bentley, S. J., Chen, Q., Edmonds, D. A., Hagen, S. C., Lam, N. S. N., ... & McCall, A. (2016). Co-evolution of wetland landscapes, flooding, and human settlement in the Mississippi River Delta Plain. *Sustainability Science*, *11*(4), 711-731.
- Van der Molen, J. (1997). Tidal distortion and spatial differences in surface flooding characteristics in a salt marsh: implications for sea-level reconstruction. *Estuarine, Coastal and Shelf Science*, *45*(2), 221-233.
- Warner, J. C., Butman, B., & Dalyander, P. S. (2008). Storm-driven sediment transport in Massachusetts Bay. *Continental Shelf Research*, *28*(2), 257-282.
- Wolanski, E., & Elliott, M. (2015). *Estuarine ecohydrology: an introduction*. Elsevier.

- Yang, S. L., Shi, B. W., Bouma, T. J., Ysebaert, T., & Luo, X. X. (2012). Wave attenuation at a salt marsh margin: a case study of an exposed coast on the Yangtze Estuary. *Estuaries and Coasts*, *35*(1), 169-182.